Geomechanics and Engineering, *Vol. 32, No. 4 (2023) 411-426*
https://doi.org/10.12989/gae.2023.32.4.411

Dynamic shear modulus and damping ratio of saturated soft clay under the seismic loading

Zhen-Dong Cui*, Long-Ji Zhang and Zhi-Xiang Zhan

State Key Laboratory for Geomechanics and Deep Underground Engineering, School of Mechanics and Civil Engineering, China University of Mining and Technology, Xuzhou, Jiangsu 221116, P. R. China

(*Received October 25, 2022, Revised January 18, 2023, Accepted January 29, 2023*)

Abstract. Soft clay is widely distributed in the southeast coastal areas of China. Many large underground structures, such as subway stations and underground pipe corridors, are shallow buried in the soft clay foundation, so the dynamic characteristics of the soft clay must be considered to the seismic design of underground structures. In this paper, the dynamic characteristics of saturated soft clay in Shanghai under the bidirectional excitation for earthquake loading are studied by dynamic triaxial tests, comparing the backbone curve and hysteretic curve of the saturated soft clay under different confining pressures with those under different vibration frequencies. Considering the coupling effects of the confining pressure and the vibration frequency, a fitting model of the maximum dynamic shear modulus was proposed by the multiple linear regression method. The M-D model was used to fit the variations of the dynamic shear modulus ratio with the shear strain. Based on the Chen model and the Park model, the effects of the consolidation confining pressure and the vibration frequency on the damping ratio were studied. The results can provide a reference to the earthquake prevention and disaster reduction in soft clay area.

Keywords: bidirectional excitation; damping ratio; dynamic shear modulus; dynamic triaxial test; empirical model; seismic loading

1. Introduction

Seismic activity usually occurs instantaneously and lasts for a short period of time. In the process of earthquakes, huge energy is often released, causing strong vibrations near the surface (Yang *et al*. 2020). Strong seismic activity will lead to widespread foundation subsidence and cracks, as well as damage and collapse of buildings. The soft clay is widely distributed in the southeastern coastal areas of China. Large-scale transportation facilities and buildings in many cities, such as subway stations and underground pipe corridors, have been built in the soft clay foundation. The seismic resistance should be considered to the design of the shallow buried underground structure. The soft clay foundation has the characteristics of poor bearing performance, high compressibility, high water content and low permeability, so the dynamic properties of the soft clay play an important role in the earthquake resistance and disaster mitigation of underground structures in soft soil areas.

In the seismic design of geotechnical engineering, it is considered that the shear wave is the main reason for the damage of the structures. The seismic load can be equivalently replaced by the case that the normal stress is constant and the shear stress changes cyclically (Seed and Idriss 1971) and the simulation of the seismic shear waves can be realized by a two-way moving triaxial instrument (Gu *et al*. 2012). In previous studies, the unidirectional loading was conducted simulating the seismic loading to study the seismic dynamic characteristics of soil through a dynamic triaxial instrument. However, the stress paths of soil under the action of one-way and two-way excitation are completely different, and the effect of different excitation methods for simulating the seismic loading has been studied (Yamada and Ishihara 1983, Li 1997, Khanbabazadeh *et al*. 2022). The seismic loading was simulated by applying the shear stress in two directions at the same time (Hu *et al*. 2018). A theoretical model describing the evolutionary features of the dynamic shear modulus and the damping ratio under different confining pressures, vibration frequencies and freeze-thaw cycles was proposed and its predicted curves agree well with the experimental results (Zhou *et al*. 2022, Gu *et al*. 2022). Gu *et al.* (2017) showed that the ratio of the dynamic deviator stress to the dynamic confining pressure significantly affected the ratio of dynamic shear modulus. The shear modulus and the hysteretic damping of three sensitive clays from Canada were investigated using a combined triaxial simple shear apparatus. The experimental data indicated that the sensitivity could affect the shape of the stiffness reduction and damping curves (Mustapha *et al*. 2021, Gu *et al*. 2022, Deviprasad *et al*. 2020). Zhou *et al*. (2017, 2019) found that the increase of shear modulus and the decrease of damping ratio with increasing confining pressure for a given initial stress ratio by the large-scale cyclic triaxial tests. A modified model for rockfill based on the existing hyperbolic model was proposed to accurately estimate the nonlinear behavior.

The dynamic shear modulus and damping ratio are

*Corresponding author, Professor
E-mail: cuizhendong@cumt.edu.cn

ISSN: 2005-307X (Print), 2092-6219 (Online)

Table 1 Physical index properties of the undisturbed muddy clay

Specific gravity G_s	Density ρ (g/cm^3)	Void ratio e_0	Water content w(%)	Liquid limit w_L(%)	Plasticity limit w_P(%)	Plasticity index I_P
2.75	1.84	1.08	35.50	36.70	21.30	21.77

indispensable parameters for evaluating the dynamic properties of soil. The maximum dynamic shear modulus, dynamic shear modulus ratio and damping ratio of clay under the seismic loading were predicted by Mansour (2018). The maximum dynamic shear modulus decreased first and then increased with the depth of soil. The dynamic confining pressure triaxial test was carried out to Ningbo saturated clay, and an empirical formula was established for predicting the damping ratio related to the cyclic stress ratio, effective consolidation confining pressure, loading frequency and cyclic confining pressure (Huang *et al*. 2021). Li *et al*. (2020) found that the dynamic elastic modulus of clay decreased with the cyclic loading times increasing.

The soil dynamic shear modulus and damping ratio change with the burial depth of soil. Li *et al*. (2022) found that the deeper the soil was buried, the higher the dynamic shear modulus ratio, while the deeper buried depth would not promote the development of the damping ratio. Wu *et al.* (2019) proposed the relationship between the maximum dynamic shear modulus and the freezing temperature, water content and confining pressure for the frozen silty clay. Lin *et al.* (2018) studied that the damping ratio was less affected by the consolidation confining pressure in the long-termcyclic loading process. Dammala *et al*. (2017) found that the effective consolidation confining pressure had an opposite effect on the dynamic shear modulus and the damping ratio of the soil, while the porosity had little effect on these dynamic parameters. An empirical model of different depths and the maximum dynamic shear modulus by the resonance column test of marine soil was established by Fang *et al*. (2021). Zulkuf *et al.* (2021) found that the stiffness of the silty clay decreased with the number of cycles increasing and the dynamic shear modulus increased with the plasticity increasing.

Till now, the seismic dynamic characteristics of the saturated soft clay have been less studied, and the different consolidation confining pressures caused by different burial depths were seldom considered for the dynamic characteristics of soft clay. It is necessary to study the effect of different consolidation confining pressures on the mechanical properties of saturated soft clay. In this paper, the dynamic triaxial test was carried out to study the dynamic characteristics of saturated soft clay, considering the effects of the confining pressure and the vibration frequency. An empirical model of the maximum dynamic shear modulus was proposed. Based on the M-D model, the attenuation law of the dynamic shear modulus was analyzed, and the variations of the damping ratio with shear strain were obtained by the Chen model and the Park model, respectively.

2. Dynamic triaxial test scheme

2.1 Test apparatus and sample preparation

The dynamic triaxial instrument produced by British GDS was used for the experimental study of the dynamic characteristics of soft clay. The GDS dynamic triaxial tester can be used to perform dynamic triaxial tests and multistage loading tests, and the dynamic confining pressure can be applied to achieve the bidirectional excitation. By adjusting the loading frequency and loading waveform, the effects of various types of dynamic loads such as traffic loading, wave loading and earthquake loading can also be simulated. The maximum axial force of the test system is 5 kN, and the maximum frequency of loading is 5 Hz, with the maximum confining pressure being 2 MPa. The accuracy of the displacement and the axial force sensors is 0.07% and 0.1%, respectively.

The soil samples in this experiment were selected from saturated soft clay in Shanghai, and the undisturbed soil samples were obtained by the drilling method. The soil samples taken out is 300 mm in height and 80 mm in diameter, which were put into an iron tube and fastened with the iron wire. After being transported back from the site, the soil samples were re-wrapped with the plastic wrap, sealed with the tape, and then placed in a constant temperature curing box. In the whole process, the state of the original soil sample was maintained as much as possible and the disturbance to the soil sample was reduced. The physical and mechanical parameters of the undisturbed soft clay are summarized in Table 1.

2.2 Selection of test parameters

In this test, the phase difference between the cyclic deviator stress and cyclic confining pressure is 180°. Both the load vibration frequency and cyclic stress ratio remain the same. The constant normal stress σ_c is generated on the 45° slope of the soil sample, accompanying with the cyclically alternating shear stress $\pm\sigma_d/2$. In this way, the earthquake loading on saturated soft clay is simulated, as shown in Fig. 1.

In the dynamic triaxial tests, sine waves, bias sine waves and half sine waves were mostly used to simulate dynamic loading in laboratory tests. In order to obtain the variations of the dynamic shear modulus and damping ratio with the shear strain, the multiple stage loading after the isotropic consolidation was carried out in this test, and the loading waveform was sine wave. Additionally, two test influencing factors were controlled, including the initial consolidation confining pressure and the loading frequency.

Before applying the dynamic load to soil samples, it was necessary to perform isotropic consolidation of soil samples under different effective consolidation confining pressures. The soil depths corresponding to different effective

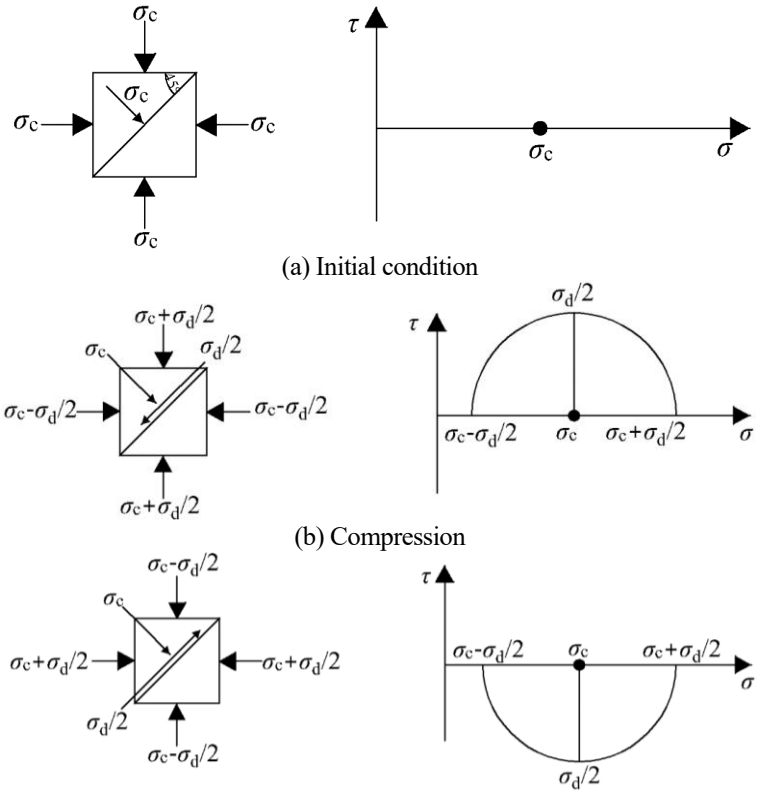

Fig. 1 Triaxial test stress state of bidirectional excitation

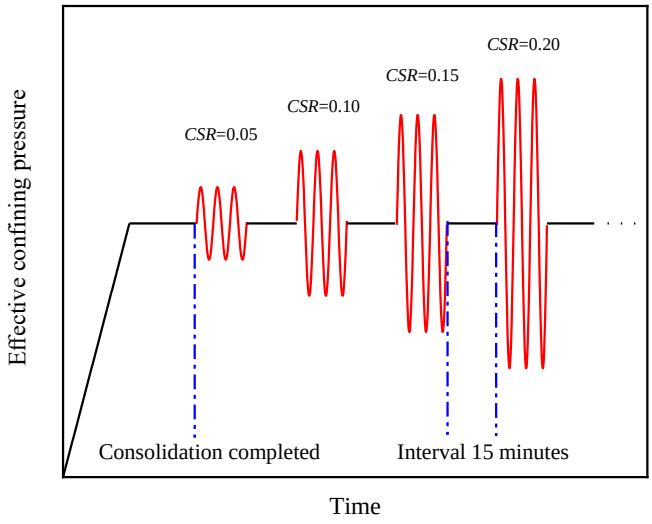

Fig. 2 Cyclic loading way

consolidation confining pressures were 3 m, 9 m, 15 m, 21 m and 27 m, respectively. The effective consolidation confining pressure at each depth was calculated by Formula (1).

$$\sigma_3^{'} = K_0\sigma_1^{'} = K_0\left(\gamma h - \psi\gamma_w h\right) \tag{1}$$

where $\sigma_1^{'}$ and $\sigma_3^{'}$ are the effective axial pressure and effective confining pressure in the consolidation stage, respectively; K_0 is the static earth pressure coefficient; γ is the soil saturation weight; h is the depth of soil layer; ψ is the lateral water pressure reduction factor, being 0.7 for clay (Cui *et al*. 2019) and γ_w is the weight of water.

The sine wave load with gradually increasing cyclic stress ratio was conducted in the multiple stage loading test. The cyclic stress ratio *CSR* was defined as

$$CSR = \sigma_d / \left(2\sigma_3^{'}\right) \tag{2}$$

where σ_d is the amplitude of cyclic stress; $\sigma_3^{'}$ is the

Table 2 Cyclic triaxial test scheme

Sample No.	Soil layer depth H (m)	Confining pressure $\sigma_3^{'}$ (kPa)	Back pressure p_b(kPa)	Frequency f (Hz)	No. of loading stages	*CSR*
C01	3	34.2	100	1	15	0.05,0.10 ,0.15,0.20,0.25 ,0.30……
C02	9	102.6	100	1	13	
C03	15	171.0	100	0.1	13	
C04	15	171.0	100	0.5	15	
C05	15	171.0	100	1	15	
C06	15	171.0	100	2	14	
C07	15	171.0	100	3	14	
C08	15	171.0	100	5	14	
C09	21	239.4	100	1	14	
C10	27	307.8	100	1	13	

effective confining pressure.

Fig. 2 illustrates the cyclic loading way and the *CSR*s are 0.05, 0.1, 0.15, 0.2, 0.25, 0.3, ……, respectively. After each stage of loading was completed, the interval was 15 minutes. For each loading stage, 3 cycles were applied on the specimen under undrained conditions, and 50 data points were saved per cycle. The dynamic properties were calculated from the second cycle data of each loading stage. With the cyclic axial strain amplitude being approximately 5%, the tests ended. The test scheme is summarized in Table 2.

2.3 Test procedure

The soft clay was cut into samples, 50 mm in diameter and 100 mm in height. Filter paper strips were sticked around the soil sample, and circular filter paper sheets were sticked both on the top and bottom of the soil sample. In order to ensure that the soil sample was in a saturated state, the back pressure saturation was conducted to the soil sample. After the sample installation was complete, each sensor was reset to zero. The back pressure was applied to the soil sample the Advanced Triaxial Test module of the GDSLAB software. The sample was completely saturated with the B value reaching 0.96 or more. After the back pressure saturation was completed, the isotropic consolidation of the sample was carried out. When the pore water pressure of the sample was equal to the back pressure and the volume change of the back pressure within 1 h was less than 0.1 cm^3, the isotropic consolidation of the sample was completed. The loading frequency, dynamic load amplitude, load waveform, and test end conditions were set by the Dynamic Cyclic Test module in the GDSLAB software. The bidirectional excitation with the sine wave load was conducted and the CSRs increased step by step being 0.05, 0.1, 0.15, 0.2, 0.25, 0.3, ……, respectively. The soil samples were characteristics of small permeability coefficient and the multiple stage loading time was very short. And the undrained conditions were chosen for the dynamic triaxial tests in this paper.

3. Analysis of dynamic triaxial test results

3.1 Hysteresis loops

Figs. 3 and 4 illustrate the hysteresis curves of saturated soft clay under different confining pressures and different frequencies, respectively. The shapes of hysteresis loops under different cyclic stress ratios are similar, but their slopes and areas are different. The area enclosed by the hysteresis curve increases significantly with the cyclic stress ratio increasing. The larger the area of hysteresis loops, the greater the energy dissipated by the soil in one loading cycle.

The area of hysteresis loop is related to the amplitude of dynamic stress. The hysteresis loop area gradually increases with the amplitude of dynamic stress increasing. The hysteresis loop is relatively steep for the small amplitude of dynamic stress. With the increase of the cyclic stress ratio, the hysteresis loop gradually slopes to the right.

The area of the hysteresis loop corresponding to the cyclic stress ratio was calculated to study the evolution law of the hysteresis curve under the multiple stage loading, shown in Fig. 5. The variations of the hysteresis loop area with the cyclic stress ratio include slow growth stage and rapid growth stage. The area of the hysteresis loop grows slowly in the first stage with the cyclic stress ratio less than 0.4, indicating that the soil energy dissipation is less at this stage. In the second stage, with the cyclic stress ratio larger than 0.4, the area of the hysteresis loop increases rapidly, and the saturated soft clay consumes more energy transferred by the dynamic load. From Fig. 5(a), the larger the effective consolidation confining pressure is, the larger the amplitude of dynamic stress corresponding to the same cyclic stress ratio is. The hysteresis loop area increases with the confining pressure and dynamic stress increasing, indicating that the soil dissipates more energy. From Fig. 5(b), in the range of 0.1 Hz~1 Hz, the increase of frequency has a repressive effect on the development of the hysteresis loop area, and the hysteresis loop area grows slowly. In the range of 2 Hz to 5 Hz, the hysteresis loop area tends to

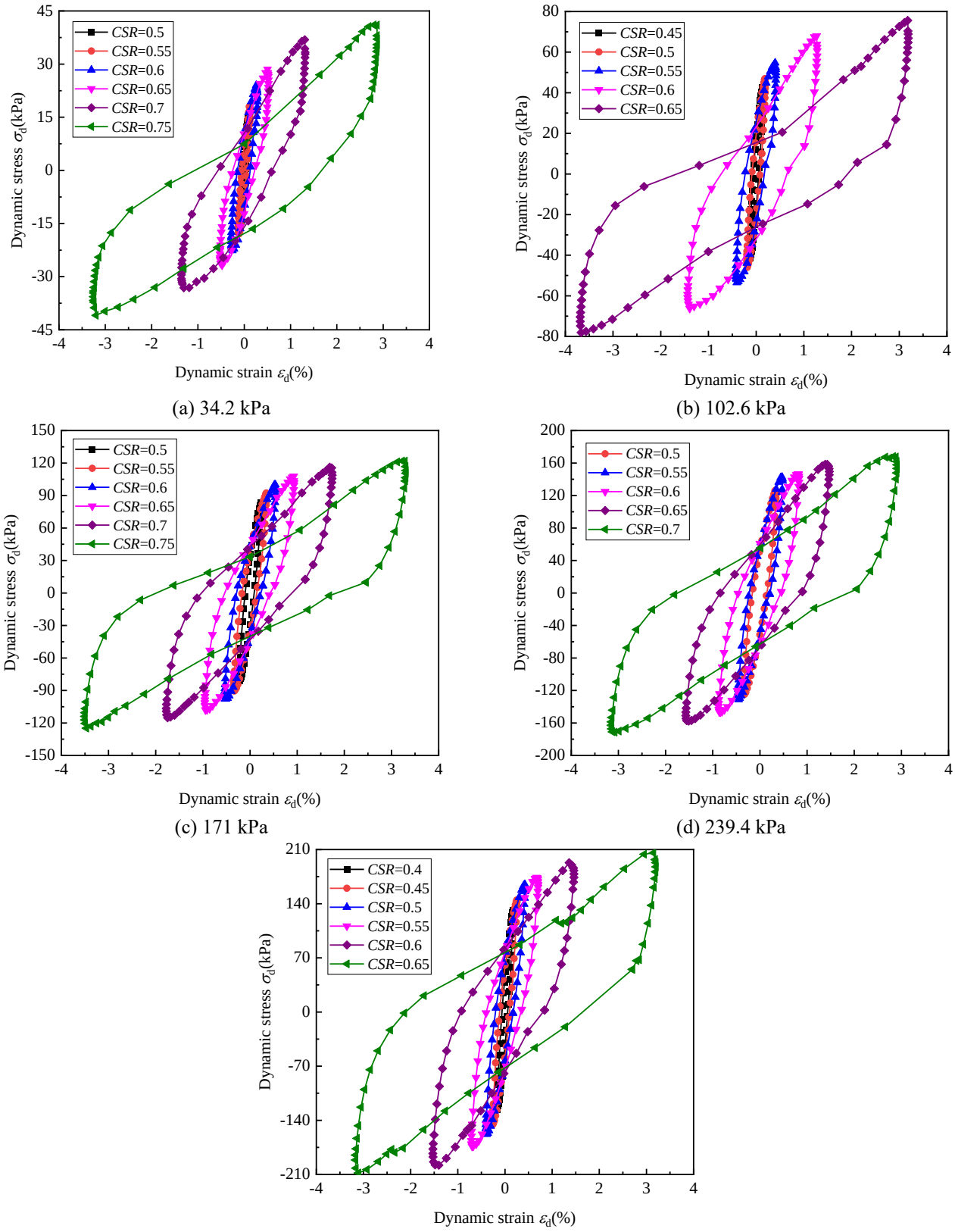

Fig. 3 Hysteresis loops of saturated soft clay under different confining pressures

decrease as the frequency increases. Especially in the second stage, the hysteresis loop area with the vibration frequency being 0.1 Hz is large than that with the frequencies being 0.5 Hz~5 Hz, whose hysteresis loop areas are close. The influence of the loading frequency on the hysteresis loop area is complex, and it is considered that

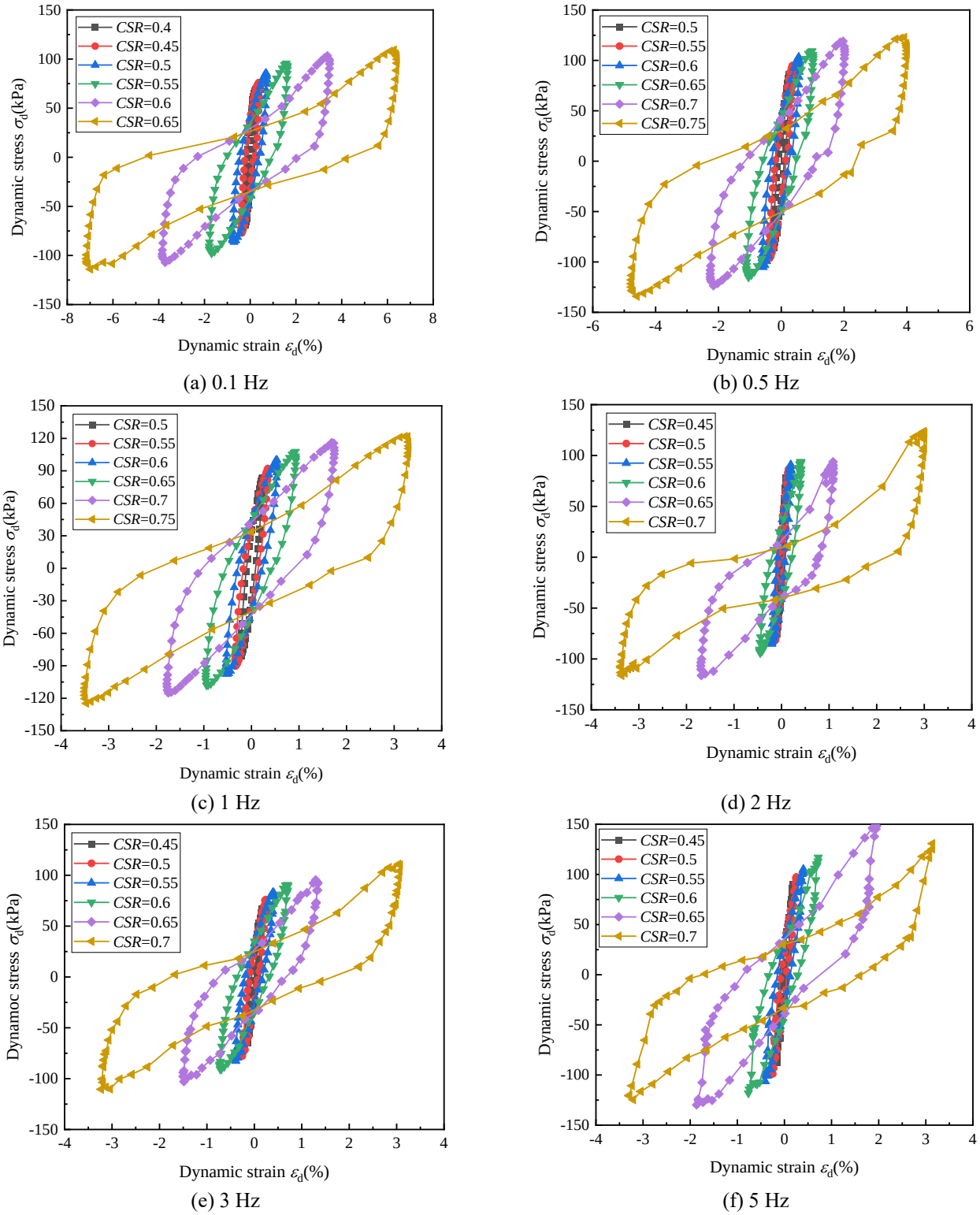

Fig. 4 Hysteresis loops of saturated soft clay under different vibration frequencies

there is a critical vibration frequency between 1 Hz and 2 Hz.

The dynamic elastic modulus of the soil can be obtained from the hysteresis curve. Fig. 6 illustrates the stiffness degradation curves of saturated soft clay. The logarithmic function shown in Formula (3) is selected for fitting the stiffness degradation curve.

$$E_d = a\ln(\varepsilon_d) + b\varepsilon_d + c \tag{3}$$

where E_d is the dynamic elastic modulus; ε_d is the axial strain; a, b and c are the fitting parameters. The test fitting parameters are summarized in Tables 3 and 4 for different confining pressures and vibration frequencies, respectively.

Table 3 Fitting parameters of soft clay stiffness degradation model under different confining pressures

Sample No.	σ_3' (kPa)	f (Hz)	a	b	c	R^2
C01	34.2	1	-5.16738	0.84774	3.72637	0.950
C02	102.6	1	-14.77779	5.04284	2.55467	0.945
C05	171.0	1	-24.76657	9.45995	1.62191	0.962
C09	239.4	1	-36.68045	17.73177	-5.57478	0.992
C10	307.8	1	-40.33325	14.79411	4.90474	0.966

Table 4 Fitting parameters of soft clay stiffness degradation model under different vibration frequencies

Sample No.	σ_3' (kPa)	f (Hz)	a	b	c	R^2
C03	171.0	0.1	-18.48513	5.47649	2.88266	0.971
C04	171.0	0.5	-23.44344	7.76642	4.11844	0.973
C05	171.0	1	-24.76657	9.45995	1.62191	0.962
C06	171.0	2	-34.63524	14.9466	-4.39241	0.953
C07	171.0	3	-22.95000	9.58675	-0.47528	0.979
C08	171.0	5	-28.69955	10.84705	2.39582	0.969

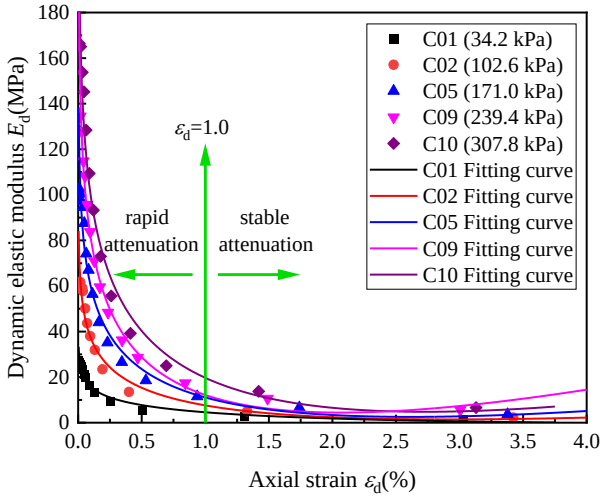

(a) Under different consolidation confining pressures

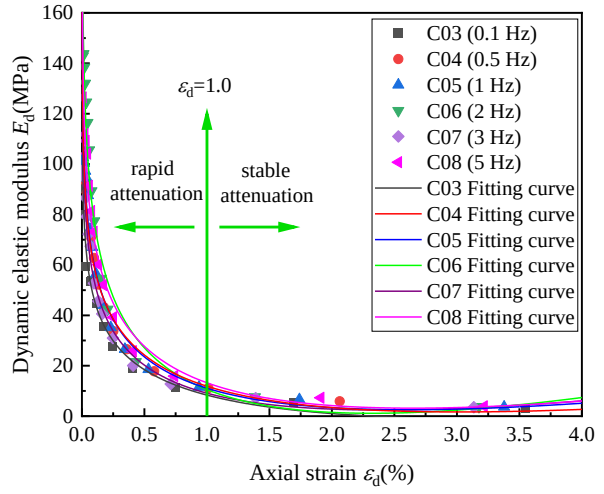

(b) Under different vibration frequencies

Fig. 6 Stiffness degradation curves of saturated soft clay

The dynamic elastic modulus of the soft clay gradually decreases with the increase of the axial strain. From Fig. 6(a), with the confining pressure increasing, the dynamic elastic modulus corresponding to the same strain is larger and the decay rate is slower, and the confining pressure has a significant effect on the stiffness degradation of the soft clay. The main reason for this phenomenon is that the consolidation effect strengthens the stiffness of the sift clay. From Fig. 6(b), the stiffness degradation curves of the soft clay almost overlap for the different frequencies, indicating that the frequency is not the dominant factor for the stiffness degradation of the soft clay. The stiffness degradation of the soft clay decreases sharply at the initial stage and then maintains an approximately constant value. The variations of the dynamic elastic modulus with the axial strain can be divided into two stages, including rapid attenuation and stable attenuation. The dynamic elastic modulus declines rapidly at first with the axial strain less than 1.0. Subsequently, with the axial strain larger than 1.0, the dynamic elastic modulus decreases slowly.

3.2 Backbone curves

The backbone curve reflects the relationship between the maximum dynamic stress and the maximum dynamic strain in each cyclic load action period of the soil under different cyclic stress ratios. Fig. 7 shows the backbone curves of soil under different confining pressures and vibration frequencies, respectively. The nonlinearity of the backbone curves shows the nonlinear relationship between the stress and the strain for the dynamic loading. In the early stage of cyclic loading, the slope of the backbone curve is very large, and the dynamic strain develops slowly, while the dynamic stress develops rapidly. As the dynamic strain increases, the backbone curve tilts to the right, indicating that the slope of the backbone curve decreases.

Table 5 The fitting parameters of backbone curves under different confining pressures

Sample No.	σ_3' (kPa)	E_0	σ_{ult}	R^2
C01	34.2	261.4995	41.0904	0.9912
C02	102.6	736.1483	73.9787	0.9915
C05	171.0	1236.7847	121.0151	0.9972
C09	239.4	1595.0532	169.9223	0.9975
C10	307.8	2051.9238	205.9051	0.9972

Table 6 The fitting parameters of backbone curve test under different vibration frequencies

Sample No.	σ_3' (kPa)	f (Hz)	E_0	σ_{ult}	R^2
C03	171.0	0.1	805.76245	106.30327	0.9915
C04	171.0	0.5	1184.79519	123.56203	0.9985
C05	171.0	1	1236.78465	121.01507	0.9972
C06	171.0	2	2163.00275	113.01147	0.9639
C07	171.0	3	1100.60268	106.45807	0.9918
C08	171.0	5	1524.87128	132.00091	0.9953

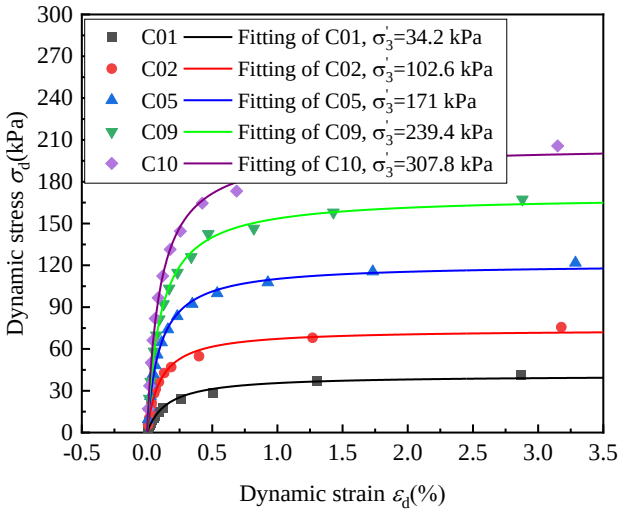

(a) Under different confining pressures

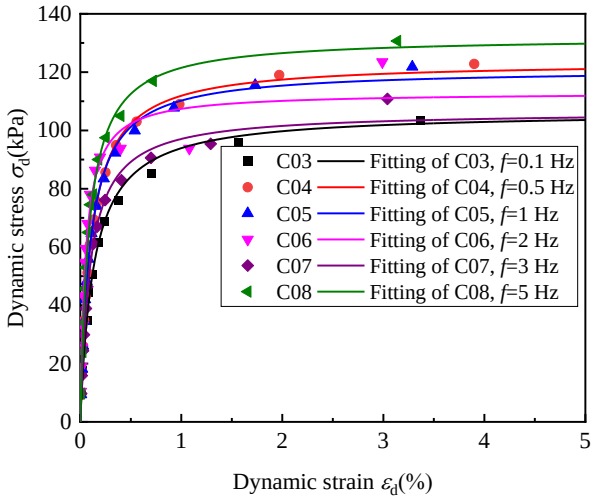

(b) Under different vibration frequencies

Fig. 7 Backbone curves of saturated soft clay

The dynamic strain increases rapidly, while the dynamic strain basically remains stable. From Fig. 7(a), the consolidation confining pressure has a significant influence on the dynamic stress-strain backbone curve. The strengthening of the confining pressure is a principal factor for the evolutionary feature of the backbone curve. From Fig. 7(b), the effect of the vibration frequency on the backbone curves can be neglected at the initial stage, which implies that the influence of vibration frequency on the backbone curves continuously strengthens with the development of the dynamic strain.

The H-D hyperbolic model (Hardin and Drnevich 1972) has a better fitting effect on the backbone curve of saturated soft clay, shown in Formula (4).

$$\sigma_d = \frac{\varepsilon_d}{\frac{1}{E_0} + \frac{\varepsilon_d}{\sigma_{ult}}} \tag{4}$$

where σ_d is the dynamic stress; ε_d is the dynamic strain; E_0 is the deformation modulus; σ_{ult} is the reference dynamic stress.

Formula (4) was used to fit the backbone curves of saturated soft clay under the different confining pressures and different vibration frequencies. From Fig. 7, the H-D model has a good fitting effect on the saturated soft clay, and the backbone curves under different confining pressures and different vibration frequencies are all “L” shaped. Within the smaller dynamic strain, the dynamic stress increases agreeing with a linear upward trend, and the soft clay is in the elastic state. Within the larger dynamic strain, the dynamic stress gradually tends to be stable, and the soil is in the plastic strain state. By comparing the effect of the effective consolidation confining pressure on the saturated soft clay backbone curve, it can be found that the initial

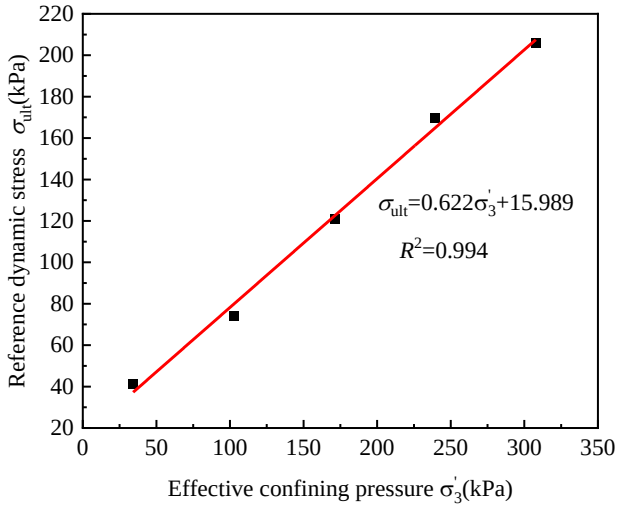

(a) Reference dynamic stress

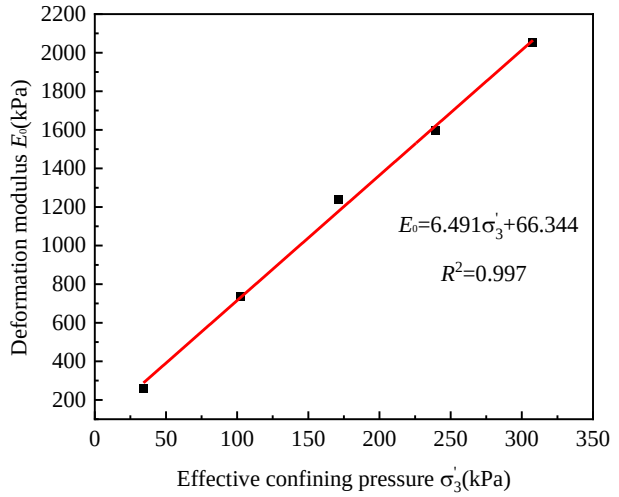

(b) Deformation modulus

Fig. 8 Fitting curve of the reference dynamic stress and deformation modulus with the effective confining pressure

slope of the backbone curve has a positive correlation with the effective consolidation confining pressure.

The parameters of fitting the backbone of saturated soft clay by the H-D hyperbolic model under different consolidation confining pressures and different vibration frequencies are summarized in Tables 5 and 6, respectively. The consolidation confining pressure has a promoting effect on the dynamic elastic modulus of the saturated soft clay. The greater the confining pressure, the greater the corresponding dynamic stress for the same dynamic strain. Taking the dynamic strain of 2.5% as an example, the corresponding dynamic stresses of the soil with effective confining pressures of 34.2 kPa, 102.6 kPa, 171.0 kPa, 239.4 kPa and 307.8 kPa are 38.7 kPa, 71.1 kPa, 116.5 kPa, 163.0 kPa and 198.0 kPa, respectively.

Under the bidirectional excitation loading, the larger the initial effective confining pressure is, the higher the soil strength is, and the less likely it is to fail. With the frequency increasing within 0.1 Hz~2 Hz, the dynamic stress corresponding to the same dynamic strain gradually

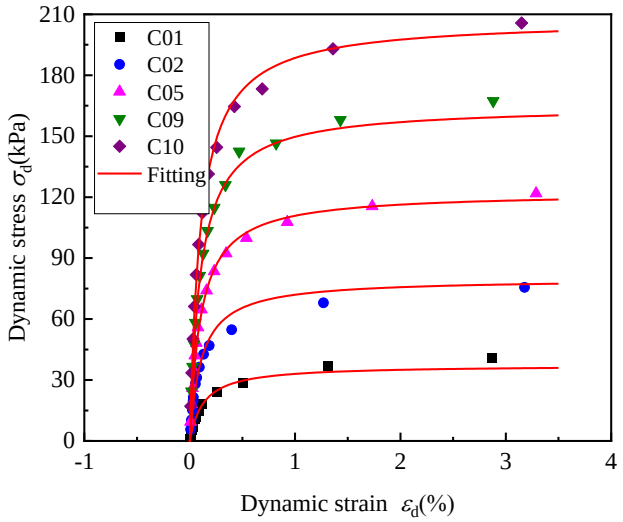

Fig. 9 Comparison of the test data with the fitting backbone curve under different confining pressures

increases. With the frequency increasing within 2 Hz~3 Hz, the dynamic stress decreases. With the frequency increasing within 3 Hz~5 Hz, the dynamic stress corresponding to the same dynamic strain increases. There is the nonlinear relationship between the frequency and the backbone curve. This is consistent with the previous analysis of frequency with the accumulated plastic strain and pore water pressure of the saturated soft clay, confirming the existence of nonlinear relationship.

Fig. 8 illustrates the variations of the reference dynamic stress and deformation modulus with the effective confining pressure, indicating the linear relationship as Formulas (5) and (6), respectively.

$$\sigma_{ult}=0.622\sigma_3^{'}+15.989 \tag{5}$$

$$E_0=6.491\sigma_3^{'}+66.344 \tag{6}$$

Based on Formulas (5) and (6), the soil backbone curves under different confining pressures are predicted, as shown in Fig. 9. The predicted soil backbone curve agrees well with the test results, which shows that it is feasible to predict the soil backbone curve through the established relationship between confining pressure and test parameters.

The H-D model is used to fit the backbone curves of the saturated soft clay under different effective confining pressures and different vibration frequencies, and there is a linear relationship between the confining pressure and the test fitting parameters of the backbone curve. The relationship between the confining pressure and the backbone curve was further obtained by fitting, and compared with the test results, it was found that the fitting effect was better.

3.3 Dynamic shear modulus and damping ratio

Fig. 10 illustrates the variations of the dynamic shear modulus ratio with the shear strain under different confining

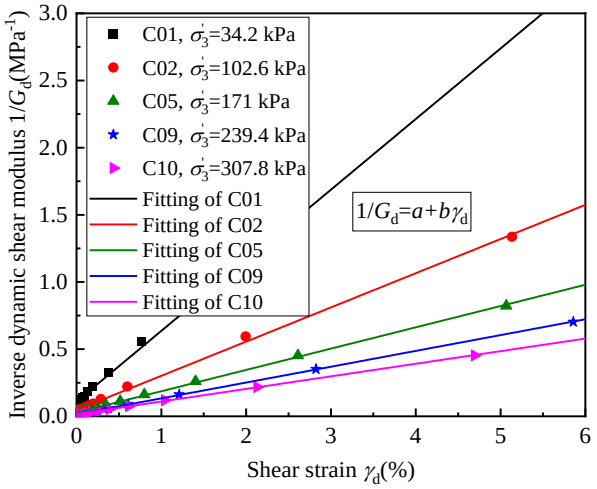

(a) Under different confining pressure

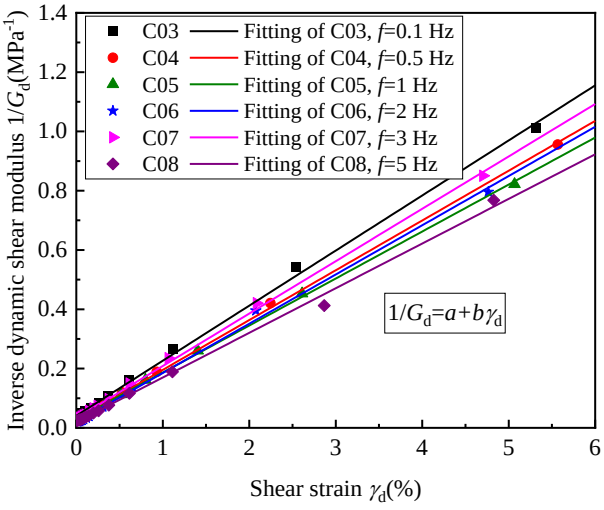

(b) Under different vibration frequencies

Fig. 10 Variations of the dynamic shear modulus ratio with the shear strain

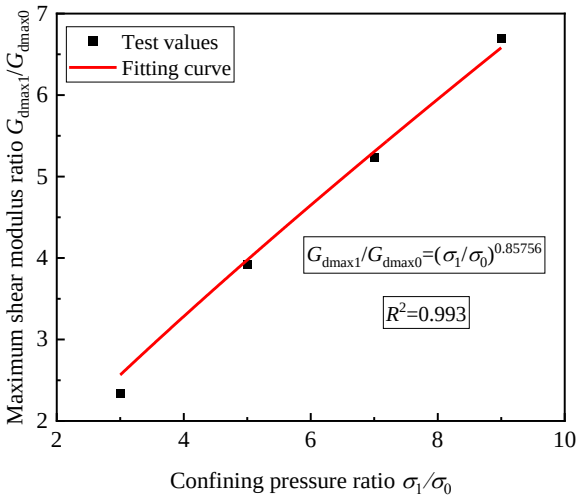

(a) Maximum dynamic shear modulus ratio

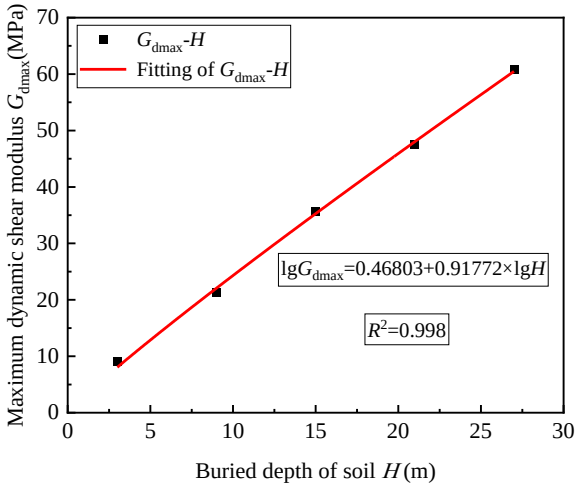

(b) Maximum dynamic shear modulus

Fig. 11 Fitting curves for the of maximum dynamic shear modulus ratio and the maximum dynamic shear modulus

pressures and different loading frequencies obtained from the multistage cyclic test, respectively. The parameters a, b and the maximum dynamic shear modulus G_{dmax} (Hardin and Drnevich 1972, Martin and Seed 1982) are obtained by fitting the test data. As the consolidation confining pressure increases, the slope and intercept of the fitting curve between the reciprocal dynamic shear modulus and the shear strain test results gradually decrease. The decrease of the intercept indicates that the larger the effective consolidation confining pressure is, the larger the maximum dynamic shear modulus of the saturated soft clay is. The increase of vibration frequency will cause the development trend of the maximum dynamic shear modulus of saturated soft clay to increase first and then decrease.

The relationship between the maximum dynamic shear modulus $G_{d\max 0}$ of the soil with the reference confining pressure σ_0 and the maximum dynamic shear modulus $G_{d\max 1}$ under the confining pressure studied by Jiang and Xing (2007) was expressed as $G_{d\max 1}/G_{d\max 0}=(\sigma_1/\sigma_0)^n$.

In this paper, the reference confining pressure σ_0 is 34.2 kPa, the fitting curve is shown in Fig. 11(a), with n being 0.8576.

The fitting relationship between soil burial depth and maximum dynamic shear modulus through experimental research on undisturbed clay was put forward as Formula (7) (Tan *et al*. 2015).

$$\lg G_{d\max}=a+b\times\lg H \tag{7}$$

where H is the burial depth of soil; a and b are the test fitting parameters.

The dynamic triaxial test under different confining pressures corresponding to different soil burial depths was carried out in this paper, and the test values of the maximum dynamic shear modulus of different buried depths of soil were fitted with the buried depth of the soil through Formula (7), shown in Fig. 11(b). It can be seen that the burial depth has a significant effect on the maximum dynamic shear modulus of the soil. The greater the burial depth, the greater the maximum dynamic shear modulus is. There is a strong linear relationship between the

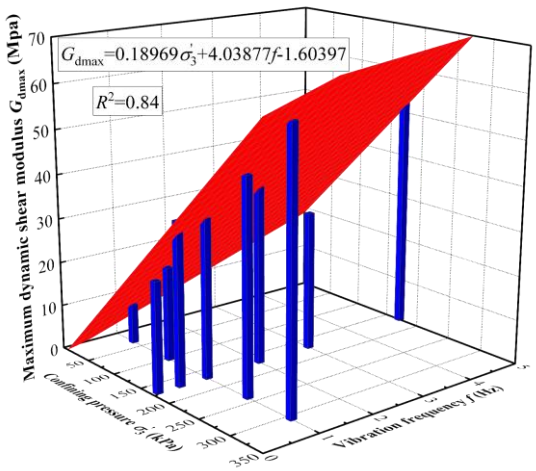

(a) Multiple linear regression model

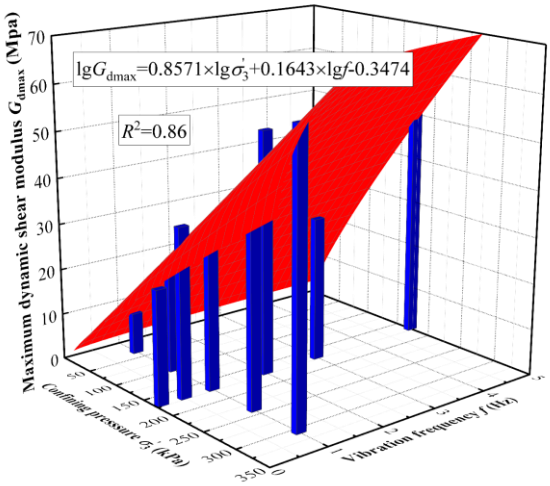

(b) Logarithmic model

Fig. 12 Variations of maximum dynamic shear modulus with confining pressure and frequency

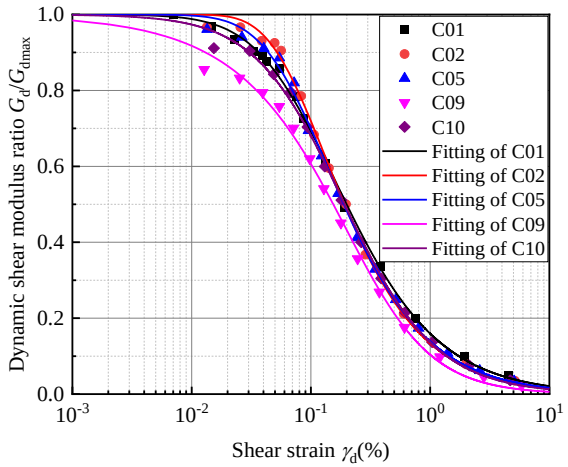

(a) Under different confining pressure

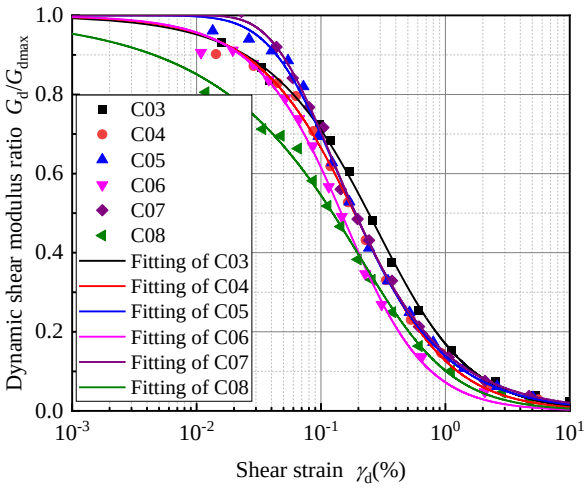

(b) Under different vibration frequencies

Fig. 13 Variations of dynamic shear modulus ratio with shear strain of saturated soft clay

burial depth and maximum dynamic shear modulus. This is because the increase of burial depth leads to a decrease in the void ratio of soil samples and an increase in the contact area between soil particles. The connection between soil particles is more closely, which leads to the faster propagation of seismic shear wave, so the maximum dynamic shear modulus also increases.

In Formula (7), the effect of vibration frequency on the maximum dynamic shear modulus was not considered. However, the maximum dynamic shear modulus was related to the different effective confining pressures and vibration frequencies, which was studied in this paper. According to the test results, the relationship among the confining pressure, the vibration frequency and the maximum dynamic shear modulus was drawn in the 3D coordinate system fitted by the method of multiple linear regression shown in Fig. 12(a). In order to find a model with a relatively good fitting effect, the logarithm of the maximum dynamic shear modulus, confining pressure and vibration frequency were obtained by referring to Formula (7), and the multiple linear regression fitting was performed as shown in Fig. 12(b). Comparing the fitting effect of the general multiple linear regression model with the logarithmic model through the correlation coefficient level R^2, it is found that the logarithmic value of the variables is better fitted on the basis of the multiple linear regression model. Compared with the multiple linear regression model, the logarithmic model has a better fitting effect on the maximum dynamic shear modulus in the lower frequency range. The combination of multiple linear regression and logarithmic model can well predict the relationship between consolidation confining pressure, vibration frequency and maximum dynamic shear modulus of saturated soft clay.

The M-D model (Martin and Seed 1982) shown in Formula (8) was used to fit the variations of the dynamic shear modulus ratio with shear strain of saturated soft clay shown in Fig. 13. The parameters of the fitting model are summarized in Tables 7 and 8.

$$G_d / G_{dmax} = 1 - \left\{ \frac{(\gamma_d / \gamma_0)^{2B}}{1 + (\gamma_d / \gamma_0)^{2B}} \right\}^A \tag{8}$$

where A and B are the fitting parameters; γ_0 is the reference shear strain; G_{dmax} is the maximum dynamic shear modulus.

Table 7 Fitting parameters for M-D model under different confining pressures

Sample No.	Depth (m)	σ_3' (kPa)	f (Hz)	$G_{d\max}$ (MPa)	M-D model parameters			
					A	B	γ_0	R^2
C01	3	34.2	1	9.08	2.38826	0.46375	0.06168	0.998
C02	9	102.6	1	21.28	15.16133	0.48164	0.00797	0.997
C05	15	171.0	1	35.60	4.31337	0.48000	0.03060	0.997
C09	21	239.4	1	47.53	0.56078	0.64822	0.30674	0.995
C10	27	307.8	1	60.83	1.21247	0.54230	0.15100	0.997

Table 8 Fitting parameters for M-D model under different vibration frequencies

Sample No.	Depth (m)	σ_3' (kPa)	f (Hz)	$G_{d\max}$ (MPa)	M-D model parameters			
					A	B	γ_0	R^2
C03	15	171.0	0.1	24.55	0.68096	0.60837	0.38595	0.998
C04	15	171.0	0.5	36.23	0.82780	0.59412	0.23387	0.997
C05	15	171.0	1	35.60	4.31337	0.48000	0.03060	0.997
C06	15	171.0	2	52.55	0.76515	0.69092	0.19326	0.997
C07	15	171.0	3	31.36	185.4626	0.44386	0.00035	0.997
C08	15	171.0	5	52.33	0.38240	0.66236	0.42728	0.995

From Fig. 13(a), the test scatters of the dynamic shear modulus ratio under different confining pressures are approximately consistent with the fitting curve simulated by M-D model. The dynamic shear modulus ratio and the shear strain of saturated soft clay show the nonlinear decreasing trend, and the overall slope of the curve first increases and then decreases. The evolutionary feature of $G_d / G_{d\max} \sim \gamma_d$ is divided into three stages: the smooth transition, the rapid attenuation and the stable attenuation. When $\gamma_d < 0.06\%$, the change of dynamic shear modulus ratio $G_d / G_{d\max}$ is not obvious, and the curve is relatively gentle; when $0.06\% < \gamma_d < 0.6\%$, the dynamic shear modulus ratio $G_d / G_{d\max}$ decays rapidly with the increase of shear strain; when $\gamma_d > 0.6\%$, the decay of dynamic shear modulus ratio $G_d / G_{d\max}$ is gradually stabilized. With the gradual increase of shear strain, the difference of dynamic shear modulus ratios of soft clays under different consolidation confining pressures gradually decreases, and finally almost coincides. When the shear strain is the same, the dynamic shear modulus ratio of soft clay first increases and then decreases with the increase of confining pressure, but the overall difference is small. It shows that the effect of consolidation confining pressure on the nonlinear characteristics of the dynamic stress-dynamic strain relationship of soft clay is not significant.

Compared with $G_d / G_{d\max} \sim \gamma_d$ of saturated soft clay under different consolidation confining pressures, the influence of different vibration frequencies on the ratio of dynamic shear modulus is more significant shown in Fig. 13(b). With the frequency increasing within 0.1 Hz~2 Hz, the dynamic shear modulus ratio of saturated soft clay decreases. From Table 8, the maximum dynamic shear modulus of saturated soft clay gradually increases within the range of 0.1 Hz to 2 Hz. For the vibration frequency within 2 Hz~3 Hz, the maximum dynamic shear modulus and dynamic shear modulus ratio of soft clay decrease with vibration frequency increasing. For the vibration frequency within 3 Hz~5 Hz, the dynamic shear modulus ratio and the maximum dynamic shear modulus increase again. It can be seen that the effect of vibration frequency on the dynamic shear modulus of saturated soft clay is complex and the regularity is not clear. It is speculated that there is a nonlinear relationship between the vibration frequency and the dynamic shear modulus of saturated soft clay.

A large number of experimental studies have been conducted on the relationship between the damping ratio and the shear strain, the empirical model of damping ratio and dynamic shear modulus ratio was established. The H-D model was applied to fit and analyze the damping ratio and the shear strain of the clay. The functional relationship of the model is as follows.

$$\lambda = \lambda_{\max}\left(1 - \frac{G_d}{G_{d\max}}\right)^m \tag{9}$$

where $\lambda_{\max}$ is the maximum damping ratio of the soil, which is treated as a test fitting parameter; m is the shape coefficient of $\lambda \sim \gamma_d$.

A large number of resonance column test data were analyzed and the damping ratio equation was optimized by Chen *et al.* (2022).

$$D = D_{\min} + D_0\left(1 - \frac{G_d}{G_{d\max}}\right)^n \tag{10}$$

where n, D_D and D_{min} are the fitting parameters. Substitute Formula (8) into Formula (10) to yield the relationship between the damping ratio and the shear strain.

$$D = D_{\min} + D_0\left(\left\{\frac{(\gamma_d/\gamma_0)^{2B}}{1+(\gamma_d/\gamma_0)^{2B}}\right\}^A\right)^n \tag{11}$$

The polynomials including dynamic shear modulus ratios were chosen to express the relationship between the damping ratio and the shear strain. An empirical expression for the damping ratio and the dynamic shear modulus ratio was proposed by Park (1998).

$$\lambda = a\left[b\left(\frac{G_d}{G_{d\max}}\right)^2 - c\left(\frac{G_d}{G_{d\max}}\right)+1\right] \tag{12}$$

where a, b and c are the test fitting parameters. Formula (8) was substituted into the Formula (12) to obtain the relationship between the damping ratio and the shear strain.

$$\lambda = a\left(b\left[1-\left\{\frac{(\gamma_d/\gamma_0)^{2B}}{1+(\gamma_d/\gamma_0)^{2B}}\right\}^A\right]^2 - c\left[1-\left\{\frac{(\gamma_d/\gamma_0)^{2B}}{1+(\gamma_d/\gamma_0)^{2B}}\right\}^A\right]+1\right) \tag{13}$$

Model parameters γ_0, A and B can be directly referred to the model fitting parameter results of each group of tests in Table 8. According to Formulas (11) and (13), the variations curves of the damping ratio and the shear strain under different consolidation confining pressures and different vibration frequencies were fitted by two models, respectively. Figs. 14 and 15 illustrate the fitting curves of the two models, and the parameters of the models are shown in Tables 9 and 10, respectively.

From Fig. 14, the overall slope of the $\lambda \sim \gamma_d$ curve first increases and then decreases. With the shear strain increasing, the evolutionary feature of damping ratio evolutionary is divided into three stages, including the slow rise, the rapid increase and finally being stable. When $\gamma_d < 0.02\%$, the variation of the damping ratio is not obvious, and the $\lambda \sim \gamma_d$ curve is relatively smooth; when $0.02\% < \gamma_d < 0.5\%$, the damping ratio increases rapidly with the increase of shear strain; when $\gamma_d > 0.5\%$, the damping ratio gradually tends to be stable. In the initial stage of multistage cyclic loading, the stiffness of the soil is large and the deformation of the soil is small. With the increase of the number of cyclic loads and the increase of the cyclic stress ratio, the soil particles begin to appear dislocation and fragmentation in a wide range. The plastic deformation of the soil sample gradually increases and the stiffness of soil decreases. Consequently, the contact points of soil particles reduce, and the pores among the soil increase, with the volume deformation of the soil gradually increasing. The dissipation of external action energy becomes more prominent, which is manifested as an increase in the damping ratio of soil.

Different from the $G_d / G_{d\max} \sim \gamma_d$ which is little affected by the consolidation confining pressure, the $\lambda \sim \gamma_d$ varies significantly with the increase of the confining

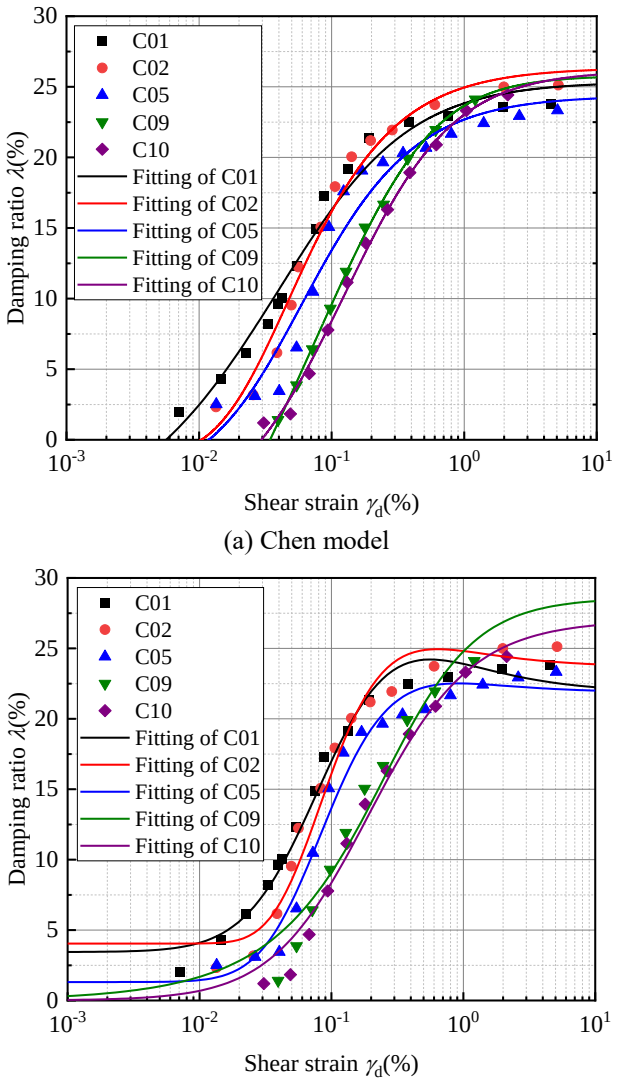

(a) Chen model

(b) Park model

Fig. 14 Variations of damping ratio with shear strain under different consolidation confining pressures

pressure. When the shear strain is small, as the confining pressure increases, the damping ratio corresponding to the same shear strain is smaller. This is because the initial void ratio of soft clay under higher confining pressure is smaller.

The continuous application of dynamic loads leads to denser soil particles, more contact points among soil particles and fewer pores. The conduction efficiency of dynamic load in saturated soft clay is higher, which is more conducive to the transmission of energy. With the increase of consolidation confining pressure, the curve of damping ratio and shear strain moves downward to the right, which also shows that the hysteresis of soil is weakened. With the further increase of shear strain, the damping ratio of soft clay with lower consolidation confining pressure gradually tends to be stable. However, the damping ratio of soil with larger consolidation confining pressure still has a tendency to increase before the failure of the sample due to the influence of the larger confining pressure compaction before. The larger the confining pressure, the larger the damping ratio corresponding to the same shear strain.

Table 9 Fitting parameters for damping ratio-shear strain model under different confining pressures

Sample No.	Depth (m)	σ_3' (kPa)	Chen model				Park model			
			D_{min}	D_0	n	R^2	a	b	c	R^2
C01	3	34.2	-6.790	32.146	0.281	0.976	3.441	-10.772	-16.128	0.983
C02	9	102.6	-1.177	27.523	0.363	0.978	4.041	-8.027	-12.887	0.965
C05	15	171.0	-2.600	26.969	0.434	0.944	1.311	-22.321	-38.006	0.971
C09	21	239.4	-45.645	71.430	0.276	0.999	0.006	1413.132	-3052.103	0.942
C10	27	307.8	-6.712	32.853	0.680	0.994	0.007	186.178	-3829.680	0.976

Table 10 Fitting parameters for damping ratio-shear strain model under different vibration frequencies

Sample No.	f (Hz)	σ_3' (kPa)	Chen model				Park model			
			D_{min}	D_0	n	R^2	a	b	c	R^2
C03	0.1	171.0	-3.907	33.921	0.547	0.972	0.612	-39.896	-82.961	0.985
C04	0.5	171.0	-12.806	39.409	0.508	0.982	0.006	-337.351	-4804.699	0.956
C05	1	171.0	-2.600	26.969	0.434	0.944	1.311	-22.321	-38.006	0.971
C06	2	171.0	-1.650	25.200	0.831	0.963	0.010	-233.893	-2586.496	0.962
C07	3	171.0	-3.309	26.516	0.702	0.986	0.011	-443.522	-2597.981	0.983
C08	5	171.0	-31.323	49.527	0.493	0.990	0.012	1861.952	211.678	0.948

From Table 9, the damping ratio-shear strain curve of the soft clay with the large confining pressure was better fitted by the Chen model, while the better fitting effect by Park model is for the low confining pressure. The damping ratio with small shear strain is poorly predicted by the Chen model. From Fig. 14, when $\gamma_d < 0.01\%$, the predicted value of the damping ratio by the Chen model is almost zero, which is difficult to predict the damping ratio. Although the Park model can still predict the damping ratio with small shear strain, it is difficult to guarantee the fitting effect. Additionally, the correlation coefficient level R^2 fitted by the Chen model is generally higher than that of the Park model, indicating that the Chen model is more superior and applicable to the fitting of the experimental results in this paper.

Compared with Figs. 14 and 15 shows that the influence of different load frequencies on the damping ratio-shear strain curve of the soft clay is more complicated and the influence amplitude is larger. An increase in the load frequency results in a decrease in the damping ratio of the saturated soft clay. With the load frequency increasing, the load acting time under the same number of cyclic load vibrations becomes shorter. The less energy applied to the soil sample from the outside, the less the damage to the soil, contributing to the less displacement and pores among soil particles. Therefore, the smaller the loss of energy transferred to the load, the smaller the damping ratio of the saturated soft clay.

From Table 10, with the vibration frequency within 0.1 Hz~1 Hz, the fitting effect of the Park model is better. However, with the vibration frequency within 2 Hz~5 Hz, the fitting effect of the Chen model is better. In practical applications, the two models can be combined to predict the damping ratio in the form of a piecewise function. Through the correlation coefficient level R^2, the overall fitting effect of the Chen model has better fitting effect on the damping ratio-shear strain curve under different vibration frequencies than that of the Park model.

4. Conclusions

A series of cyclic triaxial tests were carried out to obtain the relationship of $G_{d\max} \sim H$, $G_d / G_{d\max} \sim \gamma_d$ and $\lambda \sim \gamma_d$ for the saturated soft clay. The development of dynamic shear modulus and damping ratio, hysteresis loop and backbone curve of saturated soft clay under different confining pressures and vibration frequencies were studied, respectively. The main conclusions are as follows.

(1) The H-D hyperbolic model has a better fitting effect on the backbone curve of saturated soft clay, and the relationship between the effective confining pressure and the fitting parameters of backbone curve expressed by a linear function.

(2) With the burial depth of the soft clay increasing, the maximum dynamic shear modulus increases. Considering the coupling effect of confining pressure and vibration frequency on the maximum dynamic shear modulus, the multiple linear regression was used to propose an empirical model of the maximum dynamic shear modulus.

(3) The relationship of $G_d / G_{d\max} \sim \gamma_d$ for saturated soft clay under different confining pressures and different vibration frequencies were fitted by M-D model. The confining pressure is a principal factor for the evolutionary feature of the dynamic shear modulus of saturated soft clay. Additionally, there is a nonlinear relationship between the vibration frequency and the dynamic shear modulus of saturated soft clay.

(4) With the dynamic loading applied to the soil, the structure of the soil sample is gradually destructed, contributing to the damping ratio shrinking. The Chen

model and the Park model were respectively used to fit the curve of $\lambda \sim \gamma_d$, and the Chen model is more superior and applicable to the fitting of the experimental results in this paper.

Acknowledgements

The work in this paper was funded by the national key research and development program (Grant No. 2017YFC1500702) and by the Fundamental Research Funds for the Central Universities (2015XKMS016).

References

Abdellaziz, M., Karray, M., Chekired, M., Delisle, M.C., Locat, P., Ledoux, C. and Mompin, R. (2021), "Shear modulus and hysteretic damping of sensitive eastern Canada clays", *Can. Geotech. J.*, **58**(8), 1118-1134. https://doi.org/10.1139/cgj-2020-0254.

Cui, Z.D., Zhang, Z.L., Yuan, L., Zhan, Z.X. and Zhang, W.K. (2019), Design of Underground Structures, Springer Press, Singapore. https://doi.org/10.1007/978-981-13-7732-7.

Dammala, P.K., Krishna, A.M. and Bhattacharya, S. et al. (2017), "Dynamic soil properties for seismic ground response studies in Northeastern India", *Soil Dyn. Earthq. Eng.*, **100**(2017), 357-370. https://doi.org/10.1016/j.soildyn.2017.06.003.

Deviprasad B.S. and Dodagoudar, G.R. (2020), "Seismic response of bridge pier supported on rocking shallow foundation", *Geomech. Eng.*, **21**(1), 73-84. https://doi.org/10.12989/gae.2020.21.1.073.

Fang, Y., Lv, Y.J. and Xu. D., Peng, Y. and Zhou, X. (2021), "Experimental study of the dynamic shear modulus ratio and damping ratio of the quaternary sedimentary soils in the offshore areas of the Yellow Sea", *Geofluids*., **2021**, 8374741. https://doi.org/10.1155/2021/8374741.

Gu, C., Gu, Z.Q. and Cai, Y.Q., Wang, J. and Ling, D. (2017), "Dynamic modulus characteristics of saturated clays under variable confining pressure", *Can. Geotech. J.*, **54**(5), 729-735. https://doi.org/10.1139/cgj-2016-0441.

Gu, C., Wang, J. and Cai, Y.Q., Yang, Z.G. and Gao, Y.F. (2012), "Undrained cyclic triaxial behavior of saturated clays under variable confining pressure", *Soil Dyn. Earthq. Eng.*, **40**(2012), 118-128. https://doi.org/10.1016/j.soildyn.2012.03.011.

Gu, R., Fang, Y., Jiang, Q., Li, B. and Feng, D. (2022), "Effect of the particle size on direct shear deformation of soil", *Geomech. Eng.*, **28**(2), 135-143. https://doi.org/10.12989/gae.2022.28.2.135.

Guo, L., Liu, L., Jin, H. and Fang, Y. (2020), "Long term cyclic behavior of saturated soft clay under different drainage conditions", *Soil Dyn. Earthq. Eng.*, **139**(2020), 106362. https://doi.org/10.1016/j.soildyn.2020.106362.

Hardin, B.O. and Drnevich, V.P. (1972), "Shear modulus and damping in soils design equations and curves", *J. Soil Mech. Found.*, **98**(7), 667-692. https://trid.trb.org/view/126413.

Hu, X., Zhang, Y. and Guo, L., Wang, J., Cai, Y., Fu, H. and Cai, Y. (2018), "Cyclic behavior of saturated soft clay under stress path with bidirectional shear stresses", *Soil Dyn. Earthq. Eng.*, **104**(2018), 319-328. https://doi.org/10.1016/j.soildyn.2017.10.016.

Huang, J., Chen, J. and Ke, W., Zhong, Y., Lu, Y. and Yi, S. (2021), "Damping ratio evolution of saturated Ningbo clays under cyclic confining pressure", *Soil Dyn. Earthq. Eng.*, **143**(2021), 106581. https://doi.org/10.1016/j.soildyn.2021.106581.

Huynh, V., Nguyen, T. and Nguyen, X. (2021), "Seismic analysis of soil-structure interaction: Experimentation and modeling", *Geomech. Eng.*, **27**(2), 115-121. https://doi.org/10.12989/gae.2021.27.2.115.

Jiang, T. and Xing, H.L. (2007), "Simplified calculation method for influence of confining pressure on soil shear modulus and damping ratio", *Chinese J. Rock Mech. Eng.*, **26**(7), 1432-1437 (In Chinese). https://kns.cnki.net/kns8/defaultresult/index.

Khanbabazadeh, H., Iyisan, R. and Ozaslan, B. (2022), "Seismic behavior of the shallow clayey basins subjected to obliquely incident wave", *Geomech. Eng.*, **31**(2), 183-195. https://doi.org/10.12989/gae.2022.31.2.183.

Li, X.S. (1997), "Rotational shear effects on ground earthquake response", *Soil Dyn. Earthq. Eng.*, **16**(1997), 9-19. https://doi.org/10.1016/S0267-7261(96)00032-2.

Li, Y.Y., Li, P. and Zhu, S. (2022), "The study on dynamic shear modulus and damping ratio of marine soils based on dynamic triaxial test", *Mar. Georesour. Geotec.*, **40**(4), 473-486. https://doi.org/10.1080/1064119X.2021.1908463.

Lin, B., Zhang, F. and Feng, D.C. et al. (2018), "Dynamic shear modulus and damping ratio of thawed saturated clay under long-term cyclic loading", *Cold Reg. Sci. Technol.*, **145**(2018), 93-105. https://doi.org/10.1016/j.coldregions.2017.10.003.

Mansour, M.F. (2018), "Constitutive behavior of Port-Said Clay under seismic and small strain static conditions", *Ain Shams Eng. J.*, **9**(4), 2983-2991. https://doi.org/10.1016/j.asej.2018.06.005.

Martin, P.P. and Seed, H.B. (1982), "One dimensional dynamic ground response analysis", *J. Geotech. Eng.*, **108**(7), 935-954. https://doi.org/10.1061/AJGEB6.0001316.

Park, D. (1998), "Evaluation of dynamic soil properties: strain amplitude effects on shear modulus and damping ratios", Ph.D. Dissertation, Cornell University, New York.

Seed, H.B. and Idriss, I.M. (1971), "Simplified procedure for evaluating soil liquefaction potential", *J. Soil Mech. Found. Div.*, **97**(9), 1249-1273. https://trid.trb.org/view/127844.

Tan, H.M., Fu, H.J., Mei, T.T. and Gao, Z.B. (2015), "Experimental study on the influence of buried depth on dynamic shear modulus and damping ratio of cohesive soil", *Earthq. Eng. Eng. Vib.*, **35**(6), 136-143 (In Chinese). https://kns.cnki.net/kns8/defaultresult/index.

Wu, Z.J., Zhang, D. and Zhao, T., Ma, J. and Zhao, D. (2019), "An experimental research on damping ratio and dynamic shear modulus ratio of frozen silty clay of the Qinghai-Tibet engineering corridor", *Transportation Geotech.*, **21**(2019), 100269. https://doi.org/ 10.1016/j.trgeo.2019.100269.

Yamada, Y. and Ishihara, K. (1983), "Undrained deformation characteristics of sand in multi-directional shear", *Soils Found.*, **23**(1), 61-79. https://doi.org/10.3208/sandf1972.23.61.

Yang, S., Kwak, D. and Kishida, T. (2020), "Development of seismic fragility curves for high speed railway system using earthquake case histories", *Geomech. Eng.*, **21**(2), 179-186. https://doi.org/10.12989/gae.2020.21.2.179.

Zhang, Y., Zhao, K. and Chen, G.X. (2022), "Dynamic shear modulus and damping ratio characteristics of undisturbed marine soils in the Bohai Sea, China", *Earthq. Eng. Eng. Vib.*, **21**(2), 297-312. https://doi.org/10.1007/s11803-022-2093-4.

Zhou, W., Chen, Y. and Ma, G. (2017), "A modified dynamic shear modulus model for rockfill materials under a wide range of shear strain amplitudes.", *Soil Dyn. Earthq. Eng.*, **92**(2017), 229-238. https://doi.org/10.1016/j.soildyn.2016.10.027.

Zhou, Y., Li, M., Wen, K. and Tong, R. (2019), "Stress-strain behaviour of reinforced dredged sediment and expanded polystyrenes mixture under cyclic loading", *Geomech. Eng.*, 17(6), 507-513. https://doi.org/10.12989/gae.2019.17.6.507.

Zhou, Z.W., Li, G.Y., Shen, M. and Wang, Q.Z. (2022), "Dynamic responses of frozen subgrade soil exposed to freeze-thaw

cycles", *Soil Dyn. Earthq. Eng.*, **152**(2022), 107010. https://doi.org/10.1016/j.soildyn.2021.107010.
Zulkuf, K., Ayfer, E. and Huseyin, C. (2021), "Characterization of elastic and shear moduli of adapazari soils by dynamic triaxial tests and soil-structure interaction with site properties", *Soil Dyn. Earthq. Eng.*, **151**(2021), 106966. https://doi.org/10.1016/j.soildyn.2021.106966.

GC